X-ray Studies of Canadian Galactic Plane Survey SNRs

S. Safi-Harb, M. Jackson (*U. Manitoba, Canada*), R. Kothes (*DRAO*), & T. Foster (*Brandon*)

Motivation:

•Low-surface brightness supernova remnants are important in shaping our understanding of pulsar and supernova evolution, since the population of SNRs in our Galaxy is likely to be dominated by faint objects.

•80-90% of Galactic SNRs are expected to be of type Ib/c or II--explosions of massive stars, most of which create stellar wind bubbles around them, and thus form low-surface brightness SNRs.

•The Canadian Galactic Plane Survey (CGPS) (*Taylor et al. 2003*) is a high-resolution radio survey that incorporates single-antenna data to retain sensitivity to the largest structures (such as filamentary non-thermal radio emission from SNRs).

•So far a handful SNRs have been discovered with the CGPS (*Kothes et al. 2005*).

•We have started a program to search for their X-ray counterparts with XMM-Newton, which is best for the study of low-surface brightness SNRs in the X-ray. We also used Chandra to resolve X-ray point sources in their field and search for the putative neutron star associated with the SNR.

•The 3 SNRs presented here (G85.4+0.7, G85.9-0.9, G107.5-1.5) were discovered in CGPS data. No X-ray studies of these objects have been performed earlier.

Radio Images (CGPS):

•G85.4+0.7 has a 0.4° non-thermal shell surrounded by a 0.6° thermal shell, located within an H I bubble

•G85.9-0.6 has no discernible H I features, possibly a remnant of a Type Ia SN between the local and Perseus arms

•Central X-ray emission was detected with ROSAT (contours). No sufficient counts for a spectral analysis.

Fig. 1

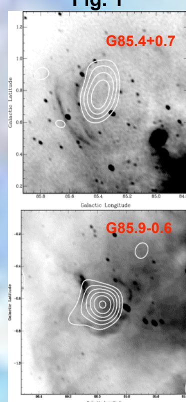

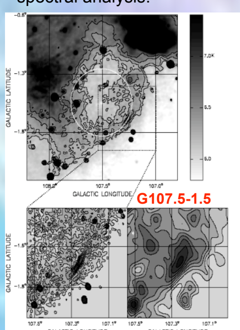

Fig.2 (left):

Top Panel: CGPS image of the highly polarized SNR G107.5-1.5 with the circle denoting the extent of the SNR.

Bottom panel: 1420 MHz and 48 MHz zoomed-on images on the radio SNR filament/shell with the white star indicating the position of an unidentified ROSAT source

Observations:

SNR G..	XMM (ks)		CXO (ks)	
	T(tot)	T(eff)	T(tot)	T(eff)
85.4+0.7	26.7	15.2	14.5	20.2
85.9-0.6	29	26	14.3	19.9
107.5-1.5	35	15	---	

Total and effective (after filtering the data for high bkg flares) exposure times with XMM and Chandra. Proton flares in XMM data have severely reduced the exposure times.

Summary:

•We detected thermal emission from G85.4 and G85.9. The SNRs appear centrally bright in soft X-rays with a thermal spectrum, and are thus classified as new Mixed-Morphology SNRs.

•G85.4 is most likely a core-collapse SN explosion but G85.9 is more likely a Type Ia explosion (enhanced Fe abundance).

•We did not detect any diffuse emission from G107.5, likely because our observation was reduced significantly by proton flares.Two soft point sources were detected near the SNR center, and coincide with an unidentified ROSAT source, that is likely the neutron star.

•Further observations are needed to better constrain the spectral parameters of the point sources, perform timing analysis of neutron star candidates, and detect diffuse emission from G107.

G85.4+0.7 and G85.9-0.6

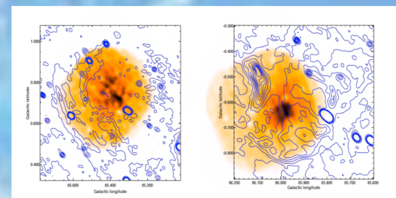

G85.4+0.7 G85.9-0.6

Fig. 3:
XMM images of G85.4 (left) and G85.9 (right) overlayed with the radio contours. The images have been smoothed with a Gaussian with σ=1' to match the radio resolution.

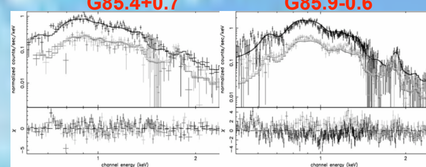

Fig. 4:
XMM-Newton spectra of the diffuse emission from G85.4 (left) and G85.9 (right). The background was subtracted locally from the same observations. See next table for a summary of the best fit model parameters, using the local bkg and the ESAS bkg.

Parameter (1)	G85.4+0.7 XMM-ESAS Background (2)	G85.4+0.7 Background Region in Fig. 2 (3)	G85.9−0.6 XMM-ESAS Background (4)	G85.9−0.6 Background Region in Fig. 5 (5)
N_H (10^{22} cm^{-2})	$0.86^{+0.04}_{-0.05}$	0.87 ± 0.06	$0.68^{+0.03}_{-0.04}$	0.70 ± 0.03
kT (keV)	$1.1^{+0.8}_{-0.3}$	$1.0^{+0.4}_{-0.2}$	$1.3^{+0.5}_{-0.2}$	$1.6^{+0.5}_{-0.3}$
τ (10^{10} cm^{-3}s)	$6.4^{+5.8}_{-2.8}$	$8.0^{+8.4}_{-3.4}$	$6.8^{+1.9}_{-0.9}$	$5.1^{+1.5}_{-1.0}$
Norm[a]	$2.4^{+0.9}_{-0.8} \times 10^{-3}$	$2.3^{+0.8}_{-0.6} \times 10^{-3}$	$1.1^{+0.1}_{-0.2} \times 10^{-3}$	$(1.1 \pm 0.2) \times 10^{-3}$
O[b]	1.2 ± 0.5	$1.2^{+2.7}_{-0.6}$	$1.5^{+0.5}_{-0.4}$	$1.7^{+0.6}_{-0.4}$
Ne[b]	$0.4^{+0.1}_{-0.3}$	$0.5^{+0.2}_{-0.4}$	$0.0^{+0.2}_{-0.0}$	$0.0^{+0.2}_{-0.0}$
Mg[b]	0.3 ± 0.1	$0.4^{+0.1}_{-0.2}$	$0.6^{+0.2}_{-0.1}$	$0.6^{+0.1}_{-0.2}$
Si[b]	0.1 ± 0.1	0.2 ± 0.2	1.1 ± 0.2	0.8 ± 0.2
S[b]	$0.4^{+0.2}_{-0.4}$	$0.8^{+1.7}_{-0.8}$	$0.8^{+0.9}_{-0.8}$	$0.4^{+0.8}_{-0.4}$
Fe[b]	$1.1^{+0.3}_{-0.2}$	$1.1^{+0.5}_{-0.3}$	$2.6^{+0.5}_{-0.2}$	2.6 ± 0.3
χ^2_ν (ν)	1.41 (209)	1.38 (211)	1.50 (460)	1.78 (465)
Distance (kpc)	3.5 ± 1.0	3.5 ± 1.0	4.8 ± 1.6	4.8 ± 1.6
Radius (pc)[c]	$(6.4 \pm 1.8)D_{3.5}$	$(6.4 \pm 1.8)D_{3.5}$	$(7.5 \pm 2.5)D_{4.8}$	$(7.5 \pm 2.5)D_{4.8}$
Temperature (MK)	13^{+9}_{-3}	12^{+5}_{-2}	15^{+6}_{-2}	19^{+6}_{-3}
0.5–2.5 keV absorbed flux[d]	1.1×10^{-12}	9.6×10^{-13}	1.5×10^{-12}	1.6×10^{-12}
0.5–2.5 keV unabsorbed flux[d]	2.7×10^{-11}	1.8×10^{-11}	1.2×10^{-11}	1.4×10^{-11}
Luminosity (0.5–2.5 keV) (erg s^{-1})[e]	$3.1^{+1.3}_{-1.5} \times 10^{33} D^2_{3.5}$	$2.0^{+1.6}_{-1.0} \times 10^{33} D^2_{3.5}$	$2.4^{+1.2}_{-1.1} \times 10^{34} D^2_{4.8}$	$2.7^{+1.2}_{-1.3} \times 10^{34} D^2_{4.8}$
n_e (cm^{-3})	$(0.11 \pm 0.03)(fD_{3.5})^{-1/2}$	$0.11^{+0.05}_{-0.04}(fD_{3.5})^{-1/2}$	$0.07^{+0.03}_{-0.02}(fD_{4.8})^{-1/2}$	$(0.07 \pm 0.03)(fD_{4.8})^{-1/2}$
t (kyr)[f]	$18^{+17}_{-9}(fD_{3.5})^{1/2}$	$23^{+26}_{-14}(fD_{3.5})^{1/2}$	$30^{+12}_{-13}(fD_{4.8})^{1/2}$	$22^{+11}_{-10}(fD_{4.8})^{1/2}$
Mass of X-ray emitting gas ($M_\odot$)	$(2.8 \pm 1.5)f^{1/2}D^{5/2}_{3.5}$	$2.8^{+1.8}_{-1.6}f^{1/2}D^{5/2}_{3.5}$	$2.7^{+1.8}_{-1.6}f^{1/2}D^{5/2}_{4.8}$	$(2.7 \pm 1.8)f^{1/2}D^{5/2}_{4.8}$

Note.—Errors are 2 σ uncertainties. Abundances of He, C, and N are frozen to solar. The Ni abundance is tied to the Fe abundance in the fits.
[a] Norm = $(10^{-14}/4\pi D^2)\int n_e n_H\, dV$ cm^{-5}.
[b] Elemental abundances are relative to solar abundance.
[c] From the X-ray extraction radius in Figs. 2 and 5; $D_{3.5}$ and $D_{4.8}$ are distances in terms of 3.5 and 4.8 kpc, respectively.
[d] Flux in erg cm^{-2} s^{-1}.
[e] The parameter f is the volume filling factor.

•Distances to the SNRs were determined using HI data and found to be: 3.5+/-1.0 kpc and 4.8+/-1.0 kpc for G85.4+0.7 and G85.9-0.6, respectively.

•Nine point sources were identified in G85.4 and another nine in G85.9.

•Based on a combination of the optical/X-ray ratios (*assuming* the optical sources are the counterparts of the X-ray srces), distances from the SNRs centres, and comparisons of N_H to that of the diffuse emission from the SNRs, none of the point sources appears a convincing neutron star candidate.

•A deeper and dedicated timing study of the pt sources, in particular for G85.4 (a most likely core-collapse SN), is needed to find its neutron star.

G107.5-1.5

Red: soft, Green: Medium, Blue: Hard

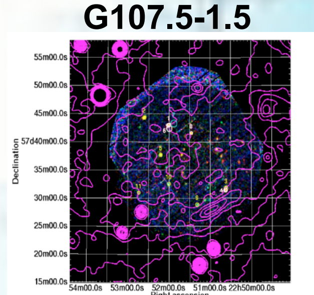

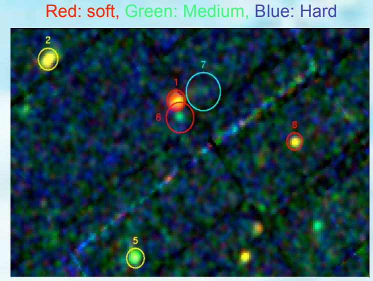

No diffuse emission was detected from the SNR.

#	N_H(10^{22}cm^{-2})	kT (keV)	0.5–5 keV Flux[a]	χ^2_ν (ν)
Absorbed blackbody				
1	$0.4^{+1.3}_{-0.5}$	$0.10^{+0.07}_{-0.05}$	0.7 (unconstrained)	1.27 (18)
	(0.6)[b]	$0.092^{+0.009}_{-0.010}$	$1.2^{+1.3}_{-0.6}$	1.21 (19)
2	$0.46^{+1.46}_{-0.46}$	$0.10^{+0.08}_{-0.05}$	> 0.3	1.38 (18)
	(0.6)	$0.092^{+0.011}_{-0.010}$	$1.3^{+1.2}_{-0.6}$	1.31 (19)
4	$2.6^{+2.6}_{-1.9}$	$0.041^{+0.041}_{-0.019}$	44700 (unconstrained)	0.54 (16)
	(0.6)	$0.086^{+0.011}_{-0.010}$	$1.2^{+1.6}_{-0.6}$	0.88 (17)
5	$0.^{+0.17}_{-0.}$	$0.86^{+0.19}_{-0.16}$	$0.084^{+0.028}_{-0.021}$	1.37 (19)
7	$2.8^{+20}_{-2.8}$	$0.04^{+1.2}_{-0.04}$	7000 (unconstrained)	0.75 (7)
	(0.6)	$0.08^{+2.6}_{-0.08}$	0.34 (unconstrained)	0.67 (8)
Absorbed power law				
	N_H(10^{22}cm^{-2})	Γ	0.5–5 keV Flux[a]	
3	$0.42^{+1.13}_{-0.42}$	$1.21^{+1.1}_{-0.76}$	$0.11^{+0.34}_{-0.07}$	1.02 (19)
	(0.6)	$1.40^{+0.45}_{-0.44}$	$0.12^{+0.05}_{-0.04}$	0.98 (20)
5	$0.^{+0.43}_{-0.}$	$0.98^{+0.68}_{-0.32}$	$0.09^{+0.10}_{-0.02}$	1.18 (19)
	(0.6)	$1.71^{+0.49}_{-0.43}$	$0.13^{+0.05}_{-0.04}$	1.56 (20)
6	$0.^{+1.6}_{-0.}$	$3.1^{+40}_{-1.3}$	0.03 (unconstrained)	1.48 (6)
	(0.6)	$6.2^{+2.5}_{-2.0}$	0.34 ± 0.13	1.50 (7)
7	$0.^{+40}_{-0.}$	$7.1^{+800}_{-7.0}$	0.05 (unconstrained)	0.78 (7)
	(0.6)	$9.5^{+1500}_{-9.4}$	0.8 ± 0.8	0.68 (8)
8	$0.003^{+1.8}_{-0.003}$	$2.4^{+11.8}_{-0.9}$	> 0.016	1.19 (5)
	(0.6)	$4.8^{+1.8}_{-1.6}$	$0.14^{+0.05}_{-0.06}$	1.22 (6)
9	$0.6^{+2.4}_{-0.6}$	$1.8^{+3.0}_{-1.4}$	$0.05^{+1.15}_{-0.04}$	0.49 (7)
10	$1.6^{+4.9}_{-1.6}$	$3.8^{+8.0}_{-2.6}$	$0.26^{+3.1}_{-0.24}$	0.42 (3)
	(0.6)	$2.7^{+1.5}_{-1.0}$	$0.07^{+0.08}_{-0.04}$	0.42 (4)
11	$3.8^{+6.6}_{-3.8}$	$5.5^{+40}_{-5.4}$	6 (unconstrained)	1.10 (1)
	(0.6)	$2.1^{+1.7}_{-1.5}$	$0.08^{+0.14}_{-0.06}$	0.66 (2)

[a] Flux is in 10^{-12}ergs/(cm^{2}s). This refers to the unabsorbed flux.
[b] A number in parentheses indicates a frozen value for the fit.

Fig. 4:

- (Left): XMM image with radio contours overlayed and pt sources identified and fitted as shown in the Table to the left. (Right): Zoomed-in image on the SNR centre. Sources 1 and 6 at the position of an unidentified ROSAT source. See Table (left) for a preliminary summary of the spectral fits to all point sources.
- A deeper observation is needed to constrain the spectral parameters, and to detect diffuse emission from the SNR.

Thanks to support by NSERC, NASA, and the Canada Research Chairs program..